# Measurement of Gas-Liquid Flows in Vertical Pipes Using Turbine Flow Meter and Conductance Sensor

## Z. Y. Tang, N. D. Jin*, Y. Y. Zhou, W. K. Ren

*School of Electrical and Information Engineering, Tianjin University, Tianjin 300072, China*
*E-mail (corresponding author): ndjin@tju.edu.cn*

### Abstract

Although turbine flow meters (TFM) have made good progress in measuring flow with accurate response characteristics in single-phase flow, TFM combined with other sensors to measure two-phase flow is still a difficult and hot issue. Due to the leakage after the collection, the flow state change and slippage between the gas and liquid phases in the pipeline after the diversion are complicated, and all these factors have a significant impact on the TFM modelling. Therefore, the meter factor models of the TFM with diverter in two-phase flows have not been thoroughly solved. Thus, this study mainly investigates the performance of TFM in gas-liquid two-phase flows combined with the rotating electric field conductance sensor (REFCS). Among them, the gas holdup is implemented through the REFCS. We examine three two-phase flows TFM models including mass model, momentum model and torque model, and analyse slip ratio, an essential parameter in the meter factor models. Subsequently, based on model tests, the evaluation finds that the Chisholm slip ratio model combined with the torque model achieved the best accuracy. Consequently, the average absolute deviation (AAD) and average absolute percentage deviation (AAPD) of total flow rate are 1.23 m$^3$/d and 7.69%.

## 1. Introduction

The research on the physical model of turbine flowmeter (TFM) for single-phase flow in industrial metering has been extensive [1], and scholars have analysed its response characteristics from the perspectives of momentum exchange [2, 3] and the airfoil theory [4, 5]. Therefore, the TFM has high accuracy in predicting single-phase flow under ideal operating conditions [6, 7].

Meanwhile, in the face of the challenges posed by the high irregularity, randomness and structural instability of the two-phase flows to the TFM, some studies have explored the TFM two-phase flows meter factor models based on volume flow rate [8], mass flow rate [9], momentum conservation [10], and torque balance [11], respectively. In addition, Masuhara et al. [12] proposed an angular momentum model based on the two-phase holdup distribution and turbine structure.

Production logging provides fluid parameters in different zones for downhole investigations on movement information and properties in and near the wellbore. So far, for production logging evaluation, the TFM is usually divided into three categories [13]: continuous [14], fullbore [15], and diverter. The TFMs with diverter are commonly used in low to medium flow rate oil wells due to the advantages of enhancing fluid uniformity [16], this paper mainly focuses on TFM using diverter. Although the diverter reduces the sensitivity of TFM to the concentration profile to a

certain extent, due to the large difference in density and viscosity between gas and liquid, there will still be interphase slippage and local uneven distribution of concentration and velocity. Hence, it is necessary to combine other sensors to explore the TFM measurement model of the two-phase flows after passing through the diverter [17, 18].

To sum up, this paper adopts a small pipe measurement strategy of TFM combined with conductance sensors to address the difficulties encountered by TFM in diverter-type well completions in the oil industry. First, in order to accurately describe the degree of slippage, with the help of the holdup provided by the REFCS, we characterize the key coefficient associated with flow patterns in the slip ratio model. Second, we assess the meter factor models including mass, momentum, and torque models through model tests. Finally, the results show that the Chisholm slip ratio model [19] combined with the torque model in this paper can effectively predict the total flow rate with the AAPD of 7.69%.

## 2. Experimental system

### 2.1 Measurement loop

As shown in Figure 1, the device is a combined measurement system of TFM and REFCS, the inner diameter is 20 mm, and the total length is 2000 mm. The medium used in the experiment was air and tap water. The specific steps are as follows: first, fix the gas flow rate to a certain value, and then gradually change the liquid flow rate to obtain a set of output signals of

TFM and REFCS, respectively. After the liquid phase flow rate is changed from the minimum to the maximum, change the gas phase flow rate and repeat the above steps. In the experiment, the variation range of gas flow rate is 1-16 m³/d, and that of liquid phase is 2-30 m³/d.
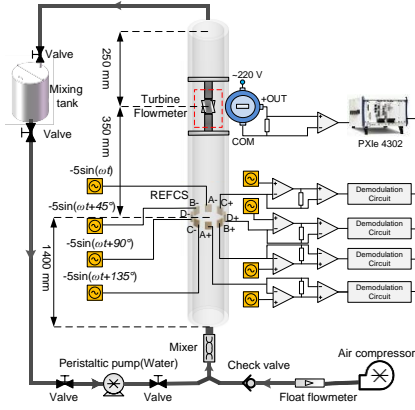


**Figure 1:** Combined measurement system.

*2.2 Turbine flow meter and conductance sensor*
The TFM utilized for the experiment is shown in Figure 2. The TFM is 1750 mm from the inlet, which is intended to ensure uniform mixing of two-phase flows and avoid experimental contingency.



**Figure 2:** Pictures of the TFM.

The REFCS is 1400 mm from the inlet. The structure diagram of REFCS [20] is shown in Figure 3.
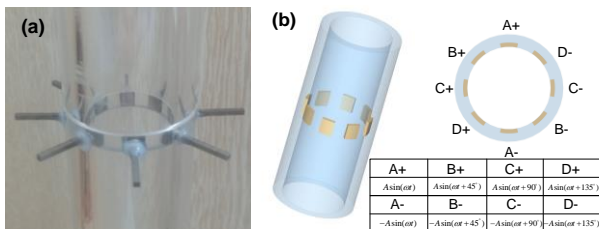


**Figure 3:** Structure of REFCS. (a) Picture of REFCS. (b) Parameters of REFCS.

There are eight electrodes in total, and two electrodes on the same diameter are a pair i.e., A-, A+, B-, B+, C-, C+, D- and D+. An electric field of equal angular frequency and 45 degrees phase difference is applied to the four

pairs of electrodes. The corresponding synthetic electric field strength is constant, and the angle rotates at the speed of $\omega$.

## 3. Measurement of gas holdup

At this time, the intensity of the synthesized electric field is constant, the angle changes with time, and the electric field rotates. The signal measured by REFCS is shown in Figure 4.

During the slug flows, the voltage value fluctuates up and down, and the interval between the peak and the trough is long, because the liquid slugs and the gas slugs appear alternately.
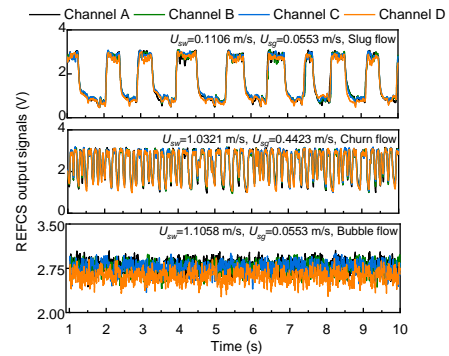


**Figure 4:** Output voltage of the REFCS.

In churn flows, the fluctuation frequency of the sensor output signal is accelerated. This is due to the fact that as the flow rate of the mixed fluid increases, the flow conditions become more complex and violent, resulting in drastic changes in voltage values. In bubble flows, the dispersed bubbles in the continuous water phase move randomly and violently. Compared with slug flows, the amplitude range of bubble flows signal is smaller, indicating that the cross-section phase distribution has better stability.

We assume that the normalized conductivity of the four channels is

$$G_e^i = \frac{\sigma_m^i}{\sigma_w} (i = A, B, C, D) \tag{1}$$

where $\sigma_m^i$ is the two-phase conductivity, $\sigma_w$ is the conductivity of pure water, and A-D respectively represent the four channels of REFCS. Then the average normalized conductivity of the four pairs of electrodes can be obtained

$$G_e^* = \frac{1}{4}(G_e^A + G_e^B + G_e^C + G_e^D). \tag{2}$$

According to Equation (2), the water holdup of bubble flow, slug and churn flows [21] can be calculated according to Maxwell assumption

$$Y_w = \begin{cases} \dfrac{3}{1+2G_e^*} & \text{Bubble flow} \\ a\dfrac{3}{1+(2/G_e^*)}+b(G_e^*)^{1.5016} & \text{Slug and churn flows} \end{cases} \quad (3)$$

$$Y_g = 1 - Y_w \quad (4)$$

where $a$ and $b$ are the weights of the high and low conductivity parts, respectively.

## 4. TFM meter factor model

### 4.1 Mass model
The mass model [9] assumes that the velocity measured by the TFM is weighted and summed according to the individual phase mass flow rate.

$$U_t = x\frac{U_{sg}}{Y_g} + (1-x)\frac{U_{sw}}{Y_w} = xU_g + (1-x)U_w \quad (5)$$

where $x$ is mass flow rate fraction. $U_t$ is the velocity measured by TFM. $U_{sg}$ and $U_{sw}$ are the superficial velocities of gas and water phases. $U_g$ and $U_w$ are the gas and water phase velocities, respectively. Combined with the slip ratio $S$, Equation (5) can be expressed as

$$\frac{U_w}{U_t} = \frac{1}{xS+(1-x)}. \quad (6)$$

Combining $Y_g$, the expression of the meter factor $K_{tp}$ in two-phase flows based on Equation (6) can be obtained

$$K_{tp} = K_o\frac{\left[Y_gS^2 + Y_w(\rho_w/\rho_g)\right]}{\left[Y_gS + Y_w(\rho_w/\rho_g)\right]\left[Y_gS + Y_w\right]} \quad (7)$$

where $\rho_w$ and $\rho_g$ are the densities of the liquid and gas phases, respectively, and $K_0$ is TFM meter factor in single-phase water.

### 4.2 Momentum model
The momentum model [10] considers that the interaction between the two phases on the blade is balanced.

$$C_gY_g\rho_g(U_g-U_t)^2 = C_wY_w\rho_w(U_t-U_w)^2 \quad (8)$$

where $C_g$ and $C_w$ are the drag coefficients of the two phases, respectively. Treat the ratio of $C_g$ and $C_w$ as 1

in the same flow. Solve the expression for $U_w$ based on the mixture density $\rho_m = Y_g\rho_g + Y_w\rho_w$

$$\frac{U_w}{U_t} = \left[1+\sqrt{\frac{\rho_w}{\rho_g}\left(\frac{\rho_m-\rho_g}{\rho_w-\rho_g}\right)}\right] \bigg/ \left[S+\sqrt{\frac{\rho_w}{\rho_g}\left(\frac{\rho_m-\rho_g}{\rho_w-\rho_g}\right)}\right]. \quad (9)$$

The meter factor $K_{tp}$ based on Equation (9) can be obtained

$$K_{tp} = K_o\frac{S+\sqrt{\dfrac{\rho_w}{\rho_g}\left(\dfrac{\rho_m-\rho_g}{\rho_w-\rho_g}\right)}}{\left[1+Y_g(S-1)\right]\left[1+\sqrt{\dfrac{\rho_w}{\rho_g}\left(\dfrac{\rho_m-\rho_g}{\rho_w-\rho_g}\right)}\right]}. \quad (10)$$

### 4.3 Torque model
The torque model [11] assumes that the two phases (gas and liquid) move separately at the same angle as single-phase flow. The torque element in two-phase flows $dM_{tp}$ can be represented by the separated flow model

$$dM_{tp} = 2\pi[\rho_gY_gU_g\{c_1U_g - \omega(1+k)\}r^3 + \rho_wY_wU_w\{c_1U_w - \omega(1+k)\}r^3]dr \quad (11)$$

where $c_1$ is determined by the blade angle $\theta$ and the root mean square radius $r_m$ ($\tan\theta/r_m = c_1$). $k$ is related to the number of blades and is called the slip factor. $\omega$ is the angular velocity. Integrating Equation (11) over the blade surface yields the two-phase flows torque $M_{tp}$

$$M_{tp} = \left\{\left[r_m(1+k)mQ_{tp}\right]/A\right\}\left[\left\{A^2\tan\theta/[(1+k)mQ_{tp}]\right\} \times \left\{\rho_gY_gU_g^2 + \rho_wY_wU_w^2\right\} - Ar_m\omega/Q_{tp}\right] \quad (12)$$

where $A$ denotes the rotor sectional area. $Q_{tp}$ and $m$ represent the two-phase volume and mass flow rate, respectively.

$$Q_{tp} = Q_g + Q_w = A(Y_gU_g + Y_wU_w) \quad (13)$$

$$m = A(\rho_gY_gU_g + \rho_wY_wU_w). \quad (14)$$

Combining Equations (12)-(14), we can get

$$\frac{Ar_m\omega}{Q_{tp}} = e_1\left[\frac{(1+aS^2)}{(1+aS)\{1-Y_g(1-S)\}}\right] - e_2\frac{r_mM_{tp}}{mQ_{tp}} \quad (15)$$

where $a = (Y_g\rho_g)/(Y_w\rho_w)$ is two-phase flow coefficient.

$e_1 = \tan\theta/(1+k)$ and $e_2 = A/[r_m^2(1+k)]$ are constants related to blade profile.

Let $f(Y_g, S) = (1+aS^2)/\{(1+aS)[1-Y_g(1-S)]\}$, then Equation (15) can be written as

$$Ar_m K_{tp} = e_1 f(Y_g, S) - e_2 \lambda_{tp} \qquad (16)$$

where $K_{tp}$ is $\omega/Q_{tp}$ and $\lambda_{tp} = (r_m M_{tp})/(mQ_{tp})$ is defined as the load factor related to the flow patterns.

## 5. Slip ratio model in vertical gas-liquid flows

As an important parameter in multiphase flow, the slip ratio is of great significance to the establishment of flow prediction model. The four slip ratio models are described below. Note that the holdups in the following models are provided by REFCS.

### 5.1 Smith model
Smith [22] proposed an expression of slip ratio

$$S = 0.4 + 0.6\sqrt{\frac{\rho_w/\rho_g + 0.4(1/x-1)}{1+0.4(1/x-1)}}. \qquad (17)$$

Equation (17) has limitations, the specific conditions are as follows: (i) 6 mm$< D <$ 38 mm. (ii) Pressure (MPa): $0.1 \leqq P \leqq 14.5$. (iii) 50 kg/s$\leqq m \leqq$ 2050 kg/s.

### 5.2 Xu and Fang model
Xu and Fang [23] suggested the slip ratio model as follows

$$S = 1 + 2Y_g^{3.5}(\frac{m^2}{gD\rho_w})^{-0.2} \qquad (18)$$

where $D$ is pipe diameter. The specific conditions are as follows: (i) 0.5 mm$< D <$ 10 mm. (ii) 40 kg/s$\leqq m \leqq$ 1000 kg/s. (iii) $6 \leqq \rho_w/\rho_g \leqq 250$.

### 5.3 Chisholm model
Chisholm [19] proposed that the gas holdup $Y_g$ can be expressed by the gas cut $K_g$

$$Y_g = C \cdot K_g \qquad (19)$$

where $C$ is relevant to the phase distribution as well as the drift velocity and mixture velocity. Based on Equation (19), Chisholm [19] proposed the slip ratio model of separated flow as follows

$$S = \frac{1}{C}\left(\frac{\rho_w}{\rho_n}\right)^{1/2} \qquad (20)$$

where $\rho_n = K_g\rho_g + K_w\rho_w$ is non-slip mixture density. From equation (20), it can be seen that in the Chisholm model [19, 24], the coefficient $C$ converges to 1 at very high flow rates. Since coefficient $C$ involves key flow parameters such as drift velocity and phase distribution coefficient, it is undoubtedly crucial to the slip ratio. Coupled with the large difference between the gas and liquid phases, we consider the effect on $C$ from the perspectives of Froude number $Fr = Q_t/(\sqrt{gD})$ and gas cut $K_g$. Figure 5 shows that the Froude number and the gas cut have a significant effect on slip ratio.
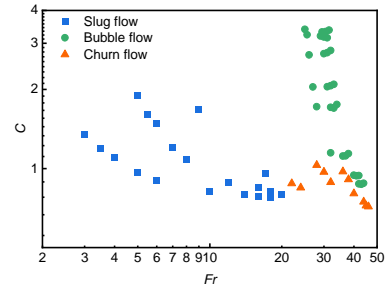
**Figure 5:** Coefficient $C$ versus $Fr$ for different flow patterns.

The coefficient $C$ is a nonlinear function of $Fr$ and $K_g$ can be obtained by multivariate nonlinear fitting

$$C = \begin{cases} 4.46Fr^{-0.21}K_g^{-0.26} & (\text{Slug flow}) \\ 9.67Fr^{-0.53}K_g^{-0.66} & (\text{Bubble flow}) \\ 24.53Fr^{-0.76}K_g^{-0.94} & (\text{Churn flow}) \end{cases} \qquad (21)$$

## 6. Results and discussions

We substitute slip ratio models in Section 5 into meter factor models in Section 4, and evaluate the accuracy of each combined model for the total flow rate.
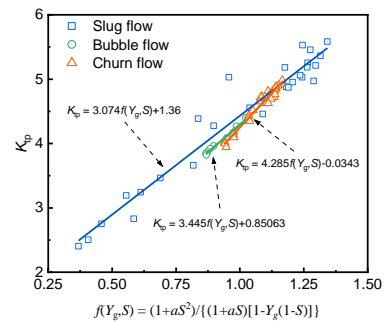
Slug flow
Bubble flow
Churn flow

$K_{tp} = 3.074f(Y_g,S)+1.36$
$K_{tp} = 4.285f(Y_g,S)-0.0343$
$K_{tp} = 3.445f(Y_g,S)+0.85063$

$f(Y_g,S) = (1+aS^2)/\{(1+aS)[1-Y_g(1-S)]\}$

**Figure 6:** Relationship between $K_{tp}$ and $f(Y_g, S)$.

In particular, it is worth noting that, for the torque model in Section 4, the specific functional relationship

between $f(Y_g, S)$ and $K_{tp}$ needs to be determined. From Equation (16), it can be seen that the $K_{tp}$ has a linear relationship with the function $f(Y_g, S)$.

It is observed from Figure 6 that there is a good linear response between $f(Y_g, S)$ and the meter factor $K_{tp}$ for different flow patterns. Therefore, we can determine the meter factor model by linear fitting

$$K_{tp} = \begin{cases} 3.074\, f(Y_g, S) + 1.36 & \text{(Slug flow)} \\ 4.285\, f(Y_g, S) - 0.0343 & \text{(Bubble flow)} \\ 3.445\, f(Y_g, S) + 0.85063 & \text{(Churn flow)} \end{cases} \quad (22)$$

To characterize the measurement error of the total flow rate, we use two metrics, i.e., the average absolute percentage (AAPD) and average absolute deviation (AAD).

$$\text{AAPD} = \frac{1}{n} \sum_{i=1}^{n} \frac{\left| Q_t^{\text{pre}} - Q_t^{\text{ref}} \right|}{Q_t^{\text{ref}}} \times 100\% \quad (23)$$

$$\text{AAD} = \frac{1}{n} \sum_{i=1}^{n} \left| Q_t^{\text{pre}} - Q_t^{\text{ref}} \right| \quad (24)$$

where $Q_t^{\text{pre}}$ and $Q_t^{\text{ref}}$ denote the predicted total flow rate and the inlet value in the $i$-th condition, respectively.
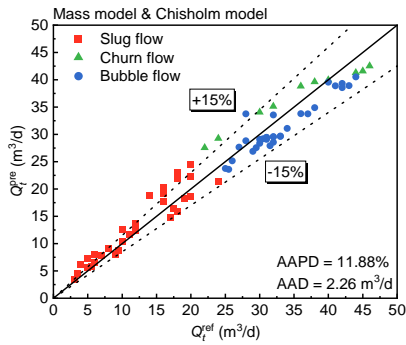


**Figure 7:** Total flow rate prediction results of mass model [9] combined with Chisholm model.

Figures 7-9 display the results of the Chisholm slip ratio model [19] combined with several TFM meter factor models to predict total flow rate. Results of other combined models are compared in Table 1. By comparison, it is found that the slip ratio model proposed in this article achieve a better performance as shown in Figure 9, especially in bubble and slug flows.

As shown in Table 1, the two indicators of the slip ratio model proposed in this paper combined with the three meter factor models are in the leading position. Among them, the combined torque model has the highest

accuracy, with AAPD of 7.6% and AAD of 1.23 m³/d. Overall, the model we designed can effectively measure the total flow rate.
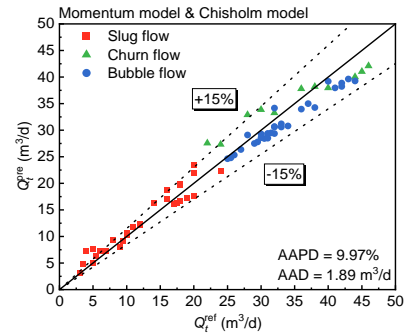


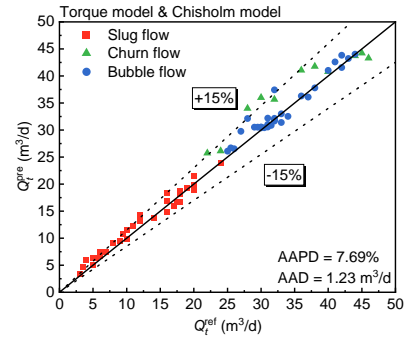**Figure 8:** Total flow rate prediction results of momentum model [10] combined with Chisholm model.



**Figure 9:** Total flow rate prediction results of torque model [11] combined with Chisholm model.

**Table 1:** Comparison of Chisholm slip ratio model with other meter factor models for total flow rate measurement.

| Slip ratio \ Meter factor | Mass model (AAD AAPD) | Momentum model (AAD AAPD) | Torque model (AAD AAPD) |
|---|---|---|---|
| **Smith model** | 2.37 m³/d 13.98% | 2.37 m³/d 13.29% | 1.91 m³/d 13.98% |
| **Xu & Fang model** | 2.54 m³/d 13.78% | 2.13 m³/d 12.85% | 1.45 m³/d 8.95% |
| **Chisholm model** | 2.26 m³/d 11.88% | 1.89 m³/d 9.97% | 1.23 m³/d 7.69% |

## 7. Conclusion

Using 20 mm inner diameter pipe, we carry out the gas-liquid flow loop test. The accuracy of flow measurement in gas-liquid flows with the TFM and conductance sensor at different slip ratio models is assessed. The contributions are summarized as follows:

(i) For gas holdup measurement, REFCS has a fast response speed that enables it to achieve satisfactory measurement accuracy using the Maxwell formula. The flow pattern identification can be satisfactorily realized based on the conductance sensor signals.

(ii) Considering the slippage effect under different flow patterns, we evaluate the model applicability of the slip ratio models, such as the Smith model, Xu and Fang model and Chisholm model. Finally, we propose an expression for the coefficient $C$ in Chisholm model with the assistance of gas holdup information and flow pattern identification. Then, we incorporate the Chisholm slip ratio model into the TFM measurement model.

(iii) We evaluated the accuracy of flow measurement with TFM and conductance sensor. Compared with TFM mass model and momentum model, the torque model has a good prediction accuracy for flow measurement of gas-liquid flows, and AAPD for prediction is 7.69%.

## Acknowledgments

## References

[1] R. C. Baker, "Turbine and related flowmeters: I. Industrial practice," *Flow Measurement and Instrumentation, 2*, pp. 147-161, 1991.

[2] W. Lee, and H. Karlby, "A study of viscosity effect and its compensation on turbine-type flowmeters," *Journal of Basic Engineering, 82*, pp. 717-725, 1960.

[3] M. Rubin, R. W. Miller, and W. G. Fox, "Driving Torques in a Theoretical Model of a Turbine Meter," *Journal of Basic Engineering, 87*, pp. 413-420, 1965.

[4] R. E. Thompson, and J. Grey, "Turbine Flowmeter Performance Model," *Journal of Basic Engineering, 92*, pp. 712-722, 1970.

[5] P. Jepson, and P. G. Bean, "Effect of Upstream Velocity Profiles on Turbine Flowmeter Registration," *Journal of Mechanical Engineering Science, 11*, pp. 503-510, 1969.

[6] R. C. Baker, "Turbine flowmeters: II. Theoretical and experimental published information," *Flow Measurement and Instrumentation, 4*, pp. 123-144, 1993.

[7] L. A. Salami, "Effect of upstream velocity profile and integral flow straighteners on turbine flowmeters," *International Journal of Heat and Fluid Flow, 5*, pp. 155-165, 1984.

[8] K. G. Turnage, and C. E. Davis, "Two-phase flow measurements with advanced instrumented spool pieces and local conductivity probes," in *Reactor Safety Instrumentation Review Group Meeting.* (Oak Ridge National Lab., TN (USA)), 1979.

[9] S. Z. Rouhani, "Application of the turbine-type flowmeters in the measurement of steam quality and void," in *Symposium on In-Core Instrumentation.* (Institutt for Atomenergi, Halden), 1964.

[10] I. Aya, *A model to calculate mass flow rate and other quantities of two-phase flow in a pipe with a densitometer, a drag disk, and a turbine flowmeter*, Oak Ridge National Lab., TN (USA), Tennessee, 1975.

[11] K. Minemura, K. Egashira, K. Ihara *et al.*, "Simultaneous Measuring Method for Both Volumetric Flow Rates of Air-Water Mixture Using a Turbine Flowmeter," *Journal of Energy Resources Technology, 118*, pp. 29-35, 1996.

[12] Y. Masuhara, M. Murase, M. Utamura *et al.*, "Evaluation Model of Turbine Meter for Two-Phase Flow," *Journal of Nuclear Science and Technology, 20*, pp. 861-867, 1983.

[13] Schlumberger, *Cased Hole Log Interpretation Principles / Applications* (Houston, Texas, Schlumberger Educational Services), 1989.

[14] J. J. Smolen, *Cased hole and production log evaluation* (Tulsa, Oklahoma, PennWell), 1996.

[15] X. X. Li, C. B. Wang, M. Wang *et al.*, "Research on Fullbore Turbine Flowmeter Application in Daqing Oilfield," *Applied Mechanics and Materials, 333-335*, pp. 263-267, 2013.

[16] Y. J. Wang, H. Y. Li, X. B. Liu *et al.*, "A new method of measuring the oil-air-water three-phase flow rate," *Chemical Engineering Communications, 207*, pp. 1-16, 2020.

[17] G. B. Zheng, N. D. Jin, X. H. Jia *et al.*, "Gas–liquid two phase flow measurement method based on combination instrument of turbine flowmeter and conductance sensor," *International Journal of Multiphase Flow, 34*, pp. 1031-1047, 2008.

[18] L. S. Zhai, N. D. Jin, Z. K. Gao *et al.*, "Well Logging Interpretation of Production Profile in Horizontal Oil-Water Two Phase Flow Pipes," *AIP Conference Proceedings*, 2012.

[19] D. Chisholm, *Two-Phase Flow in Pipelines and Heat Exchangers* (London and New York, George Godwin), 1983.

[20] D. Y. Wang, N. D. Jin, L. X. Zhuang *et al.*, "Development of a rotating electric field conductance sensor for measurement of water holdup in vertical oil-gas-water flows," *Measurement Science and Technology, 29*, pp. 075301, 2018.

[21] D. Y. Wang, N. D. Jin, L. S. Zhai *et al.*, "Salinity Independent Flow Measurement of Vertical Upward Gas-Liquid Flows in a Small Pipe Using Conductance Method," *Sensors, 20*, pp. 5263, 2020.

[22] S. L. Smith, "Void Fractions in Two-Phase Flow: A Correlation Based upon an Equal Velocity Head Model," *Proceedings of the Institution of Mechanical Engineers, 184*, pp. 647-664, 1969.

[23] Y. Xu, and X. Fang, "Correlations of void fraction for two-phase refrigerant flow in pipes," *Applied Thermal Engineering, 64*, pp. 242-251, 2014.

[24] P. V. Godbole, "Study of flow patterns and void fraction in vertical upward two-phase flow," University of Pune, University of Pune, 2009.